Pore-Fluid Quantification: Unconsolidated vs. Consolidated Sediments

Fred Hilterman, Geokinetics, USA
Zhengyun Zhou, University of Houston, USA

Abstract

The fluid factor (ΔF), Poisson Impedance (PI) and lambda-rho ($\lambda\rho$) are three seismic attributes commonly used for pore-fluid discrimination. While it is debated that one attribute is a better pore-fluid discriminator than the other, their sensitivity to pore fluid is not significantly different because the sensitivity of the three attributes are directly related to PI. In addition, the sensitivity of the three attributes is increased if attribute calibration is finalized in the horizon domain. The effectiveness of each attribute was tested for unconsolidated sediments in the Gulf of Mexico and consolidated sediments in the Southern Gas Basin of the North Sea. However, in the Paleozoic consolidated sediments of SGB, the extra sensitivity of the impedance attributes (PI and $\lambda\rho$) appear to be needed for a robust estimate of pore fluid.

Introduction

Pore-fluid and lithology prediction are two objectives in amplitude-versus-offset (AVO) analyses. Smith and Gidlow (1987) defined the fluid factor as the weighted difference between the reflectivities of P- and S-wave velocity. Goodway et al. (1997) introduced the pore-fluid attribute $\lambda\rho$ along with the lithology attribute $\mu\rho$, where $\lambda\rho$ is related to the acoustic impedance AI and shear impedance SI as $\lambda\rho = (AI)^2 - 2(SI)^2$. Hilterman (2001) and Hedlin (2000) related $\lambda\rho$ to Gassmann's pore-space modulus and Russell et al. (2003) noted that $\lambda\rho$ would be a better pore-fluid discriminator if the factor 2 in its equation relating AI and SI was varied depending on the local rock properties. Quakenbush et al. (2006) showed that the axes of the crossplot between SI vs. AI can be rotated ("pore-fluid projection") and the new attribute defined by the rotated abscissa is a good pore-fluid discriminator, which he called Poisson impedance. Our objective is to quantify the pore-fluid sensitivity of these three AVO attributes.

Two Desirable Pore-Fluid Measurements

The linear approximation of Zoeppritz's equation can be expressed as a function of the incident angle θ as

$$RC(\theta) \approx NI_{VEL}/\cos^2(\theta) + NI_{DEN} + NI_{RIG}\sin^2(\theta) \qquad (1)$$

where RC is the reflection coefficient, NI_{VEL} and NI_{DEN} are reflectivities associated with the velocity and density

variations across the interface. $NI_{RIG} = -2\Delta\mu\ \sin^2(\theta)/\rho\alpha^2$, where $\Delta\mu$ is the shear rigidity difference between the lower and upper media and ρ and α are the average velocity and density of the upper and lower media.
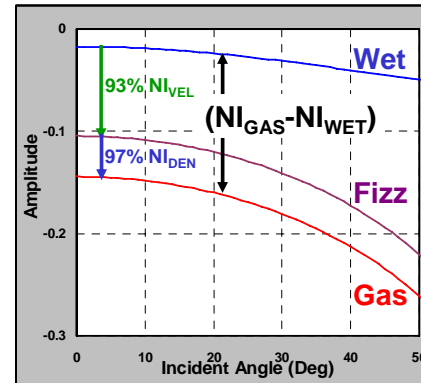

Figure 1: Zoeppritz responses for a shale over sand interface when the sand is saturated with brine, fizz (low gas saturation) and gas.

In Figure 1, the downshift of the fizz response from the wet response is primarily due to the NI_{VEL} term in equation 1 when gas is introduced. The third term with NI_{RIG} is approximately the same for all three pore fluids. Additional gas lowers the AVO Zoeppritz response to the "gas" curve. The difference between the economic gas and fizz curves is mainly caused by the changes in NI_{DEN}. The density contribution is the same at all angles during the transition from fizz to gas saturation. The discrimination of pore fluid is mainly in the measurement of (NI_{GAS}-NI_{WET}) or (NI_{FIZZ}-NI_{WET}) and not the slope. The second desired measurement is the pore-space modulus of Gassmann's equation, which is related to $\lambda\rho$. Our task is to develop seismic attributes that relate to (NI_{GAS}-NI_{WET}) and the pore-space modulus. These are investigate with well-log data first.

Well Measurements in Unconsolidated Sediments

In the northern portion of the Gulf of Mexico (GOM), velocity and density values for wet sand and shale were extracted from 150 wells at 60-m intervals. From 2700-3300-m depth, the rock properties of 183 brine-saturated reservoirs and the encasing shale were selected. These are mainly unconsolidated Pliocene-Miocene sediments. Fluid-substitution rock properties were generated for all 183 reservoirs (estimated S-wave velocity). The normal-incident P-wave (NIP) and S-wave (NIS) reflection coefficients for brine-, oil- and gas-saturations are illustrated in Figure 2a. In Figure 2b, the fluid factor is based on a rotation of the axes (ΔF=NIP-0.72NIS) while in Figure 2c the fluid factor has an additional translation term (ΔF=NIP-0.72NIS+0.03), which has an expected value of zero for the fluid factor from brine-saturated

reflections. In a similar fashion, the crossplots of (SI vs. AI) and (SI^2 vs. AI^2) were developed so that the Poisson impedance and lambda-rho attributes have expected values of zero for the wet sand as shown in Figure 3. Visual inspection of Figure 3 indicates that Poisson impedance is just as effective as lambda-rho as a pore-fluid discriminator.
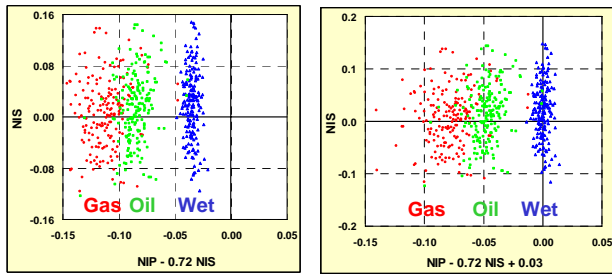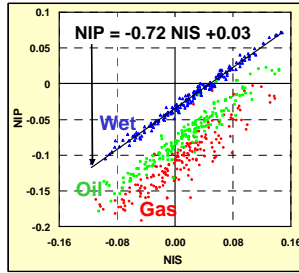

Figure 2: (a) P-wave and S-wave NI values for 183 GOM reservoirs (unconsolidated sediments), (b) fluid factor with NIP as ratio of NIS, and (c) fluid factor NIP as linear equation of NIS so that brine-saturated sands have an expected value of zero.
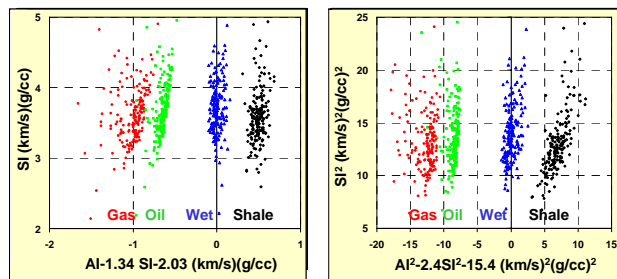

Figure 3: (a) Poisson impedance and (b) lambda-rho attributes defined so that brine-saturated sands have an expected value of zero.

When the rock properties of the three pore-fluid attributes (ΔF, PI and $\lambda\rho$) are defined as shown in Figures 2 and 3, several relationships exist. Smith and Gidlow originally defined the fluid factor as:

$$\Delta F = NIP - \gamma NIS. \qquad (2)$$

The intent was to measure the scalar γ from seismic field data so that at the top of a gas reservoir the fluid factor becomes $\Delta F = NIP(Gas)-NIP(Wet)$, which is the first desired measurement shown in Figure 1. However with well-log data, we find that a translation is actually needed to make ΔF zero for wet sand. With the translation, ΔF at the top of a gas reservoir reduces to $\Delta F \approx -NI_{GWC}$, which is the negative reflection from a gas/water contact in the reservoir (Zhou and Hilterman, in press). It is now easy to

illustrate the relationship of the three pore-fluid attributes. AI_{WET} is the acoustic impedance when the reservoir is brine saturated and AI_{GAS}, gas saturated. Let $\Delta AI = AI_{GAS} - AI_{WET}$ and $2AI = AI_{GAS} + AI_{WET}$, then the following holds

Fluid Factor	$= \Delta F = \Delta AI \times (2AI)^{-1}$	(3a)
Poisson Impedance = PI	$= \Delta AI \times (2AI)^{0}$	(3b)
Lambda-Rho	$= \lambda\rho = \Delta AI \times (2AI)^{+1}$	(3c)

In short, all three attributes consist of the sensitivity term ΔAI and a scalar term that is essentially the same for all three pore fluids. The scalar term has a different exponent for each attribute. This philosophy developed for well-log data was then tried on a 3D seismic survey in the same area as the well-log data.

Field Study in Unconsolidated Sediments

A 19 mi^2 3D seismic survey contained a producing oil and gas field with 10 wells available for our study. Seven of the oil wells were abandoned; two were still producing oil, and the last was a gas well. After AVO processing, horizon maps for NIP and NIS were generated and are shown in Figure 4.
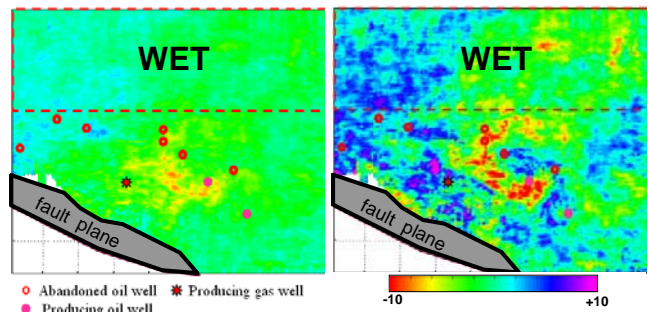

Figure 4: (a) NIP and (b) NIS horizon maps on gas-oil reservoir in unconsolidated sediments.

A disappointing interpretation feature shown in Figure 4a is that the location of the gas well is not associated with the lowest NIP amplitude (red). There are several wells in the northern portion of the area (red dashed box in Figure 4) that were brine-saturated and thus we assumed this area to be wet. From the horizon maps in Figure 4, the crossplot of NIS vs. NIP is shown in Figure 5.
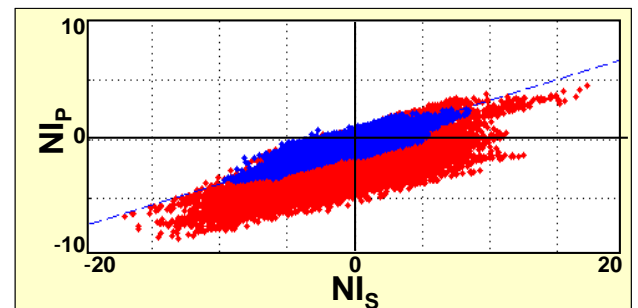

Figure 5: Horizon crossplot of NIS vs. NIP from Figure 4. Upper blue portion is from wet area in Figure 4.

The fluid factor based on the brine-saturated regression line shown in Figure 5 is

$$\Delta F = NIP - 0.35\ NIS + 25.6 \qquad (4)$$

with a high correlation coefficient $R^2 = 0.95$. One of the obvious benefits of constructing the fluid factor from a

horizon map is that a coordinate translation can be performed (+25.6) which can't be applied to a time section which has negative and positive values. The resulting fluid factor map is shown in Figure 6a. Time contours of the horizon are superimposed. This map is reasonable in that the gas well is now associated with the lowest fluid factor values and there appears to be a yellow area associated with the remaining gas zone and a green area for the remaining oil. Six of the abandoned oil wells are located on the brine-saturated blue area. There is still some discrepancy with two of the abandoned oil wells in the apparent remaining oil area. When depth contours based on the wells are superimposed, the discrepancy of a producing well being down dip from an abandoned well is resolved.
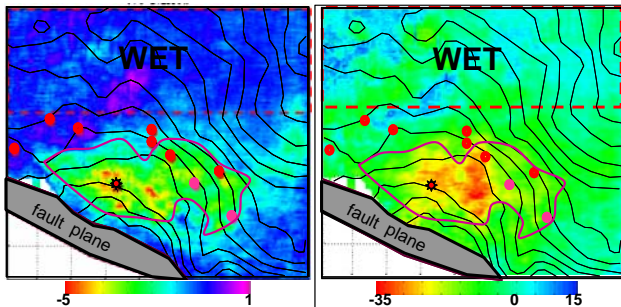

Figure 6: (a) Fluid factor and (b) PI maps across prospect.

Difficulties arose when an AI and SI inversion were attempted to develop Poisson impedance. This is an old field and even though there were ten wells, not a single well had sonic and density curves through the reservoir zone. Thus, the wavelet extractions were questionable. In addition, the reservoir is located beneath a major fault that significantly distorts the pre-stack time migration image. Though advisable, depth migration was outside the scope of this research. Thus, developing a low-frequency acoustic impedance trend for inversion was also difficult. A regional trend was used for the low-frequency.

AI and SI maps were generated and crossplotted in a fashion similar to the work for the fluid factor. The resulting Poisson's impedance map is shown in Figure 6b. A disappointing feature of the PI map is its inability to reliably discern the areas with remaining gas and oil, especially since the wells in the northern portion were dry.

A $\lambda\rho$ map was generated but it did not resolve any of the interpretation problems seen with the PI map. This was expected since the sensitivity of the PI attribute is similar to the $\lambda\rho$ attribute and both had the same limitations in the seismic inversion. The next step was to see if the concepts developed for the unconsolidated sediments could be extend to consolidated sediments.

Well Measurements in Consolidated Sediments

From twenty-five (25) wells in the Southern Gas Basin (SGB) of the North Sea, velocity and density values for sand and shale were measured in 117 Permian and

Carboniferous reservoirs. Initially, we were interested in determining what class of AVO signatures to expect in the SGB. The answer is shown by the crossplot of NIP vs. B (gradient) in Figure 7a. What is surprising is the equal distribution of Class 1, 2, 3 and 4 AVO signatures for the SGB sediments. As a means of quantifying the crossplot in Figure 7a, a similar crossplot for unconsolidated GOM sediments is depicted in Figure 7b. The unconsolidated and consolidated sediments have the same wet trend in Figure 7. The major difference between Figure 7a and 7b resides in the separation of the gas trend from the brine trend. The reflectivity difference between GOM and SGB is emphasized by comparing the fluid factor from SGB in Figure 8a to GOM fluid factor in Figure 2C. The fluid factor in Figure 8a is not a satisfactory pore-fluid discriminator. However, SGB Poisson impedance in Figure 8b is satisfactory, even when compared to the GOM PI in Figure 3a.
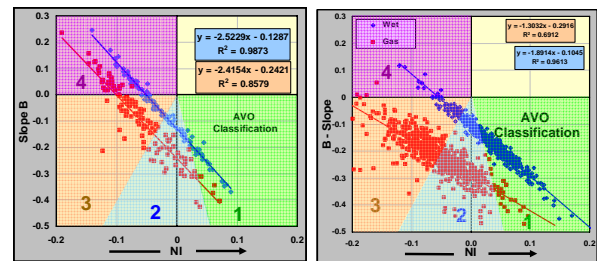

Figure 7: NI vs. B crossplots for (a) SGB consolidated sediments and (b) Gulf of Mexico unconsolidated sediments.
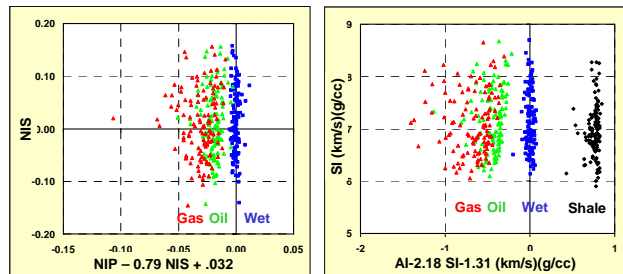

Figure 8: SGB consolidated sediment crossplots for (a) fluid factor and (b) Poisson impedance

Seismic Signatures from North Sea

The seismic signatures for the sand-shale reservoirs in the SGB are compromised by several factors. The reservoir signatures are between at least seven different dispositional sequences whose seismic signatures can override the reservoir response. A mineral volumetric analysis of a well can contain 13 primary minerals whose acoustic impedances are significant higher (anhydrite) and lower (coal) then the reservoir sand/shale impedances. This in itself is not as discerning as the influence of internal multiples below the top of the Permian. In 67% of the study wells, the seismic signature of the reservoir is overridden by internal multiple events through the pay intervals.

Numerous total wave equation synthetics were examined to help define processing algorithms that might remove

the noise components from the reservoir zone. This was successful except the internal multiples encoded in the transmitted wave remained.   While this is continuing research, we went on to investigate the primary only response for the seven different depositional settings. As an example, the AVO synthetics in Figures 9a and 9b from the Caister Field (UK44/23-4) have hydrocarbons on the left side and no hydrocarbons on the right. Figure 9a has a higher frequency wavelet than that in Figure 9b.

The AVO signature in Figure 9a is Class 4 and the ratio of NI_{GAS}/NI_{WET} is 100/98. When the wavelet frequency is reduced, the signature goes to a Class 1 with a NI_{GAS}/NI_{WET} ratio of 75/100. From this figure one might surmise the following.

- High frequency is not always the best interpretation tool for AVO.
- Phase reversals within CMP gathers are very important gas indicators in Class 1 environments.
- Offsets as large as twice the depth are needed for phase reversal recognition in Class 1 environments.
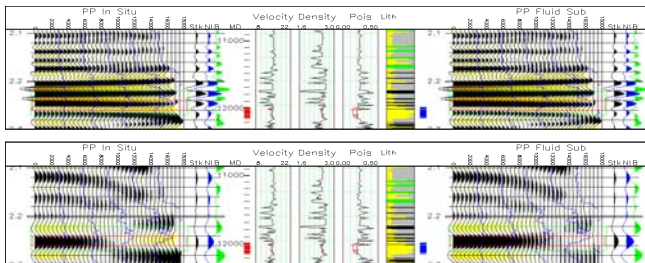- Tuned lower-frequency enhances the recognition of gas intervals.

Figure 9: (a) AVO response with in-situ hydrocarbons (left) and fluid-substitution to brine saturation (right) at 5-8-55-65 Hz wavelet; (b) Similar to (a) but with a 5-8-20-25 Hz wavelet.
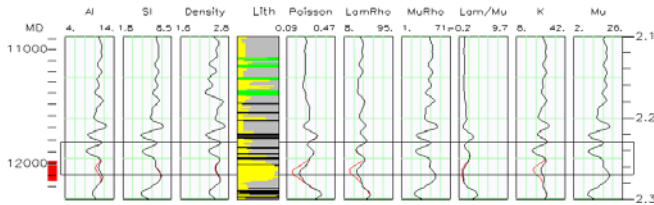

Figure 10: Impedance attributes for same well in Figure 8 with high-cut 5-8-55-65 Hz.

With the interpretation of the seismic signature dependent on the wavelet frequency, the impedance responses for the well in Figure 9 were evaluated as pore-fluid discriminators (see Figure 10).   While the reflectivity attributes might be questionable, PI and lambda-rho appear to be potential pore-fluid discriminators, much as predicted from the well-log study.

Conclusions

- The fluid factor is defined as the difference of two reflectivities. However, at the reservoir top, it equals the negative of the equivalent gas/water interface reflection. Poisson impedance (AI_{HYD}-AI_{WET}) is also

the main sensitivity term for the fluid factor and lambda-rho.
- Crossplotting horizon AVO attributes provides linear relationships rather than ratios, which increases the pore-fluid discrimination sensitivity.
- All AVO classes existed in both the consolidated and unconsolidated sediment study areas.   Pore-fluid discrimination is related to the magnitude of the fluid factor not the AVO class.
- In the consolidated sediment area, the AVO class and the ability to discriminate pore fluids in the reflectivity domain can be dependent on the wavelet frequency band.
- If adequate well-log control is not available, PI and $\lambda\rho$ attributes lose their advantage over the fluid factor.

References

Goodway, B., T. Chen, and J. Downton, 1997, Improved AVO fluid detection and lithology discrimination using Lam petrophysical parameters; lr, mr & l/m fluid stack, from P and S inversions: 67th Annual International Meeting, SEG Expanded Abstracts, 183-186.

Hedlin, K., 2000, Pore space modulus and extraction using AVO: 70th Annual International Meeting, SEG Expanded Abstracts, 1572-1575.

Hilterman, F., 2001, Seismic Amplitude Interpretation: 2001 SEG-EAGE DISC Book.

Quakenbush M., B. Shang, and C. Tuttle, 2006, Poisson impedance: The Leading Edge, 25, 128-138.
Russell, B.H., Hedlin, K. and Hilterman, F.J., 2003, Fluid-property discrimination with AVO: A Biot-Gassmann perspective: Geophysics, 68, 29-39.

Smith, G. and P. Gidlow, 1987, Weighted stacking for rock property estimation and detection of gas: Geophysical Prospecting, 35, 993–1014.

Zhou, Z. and F. Hilterman, 2007, Is there a basis for all AVO attributes?: 77th Annual International Meeting, SEG Expanded Abstracts, 244-248.

Zhou, Z. and F. Hilterman, In Press, A comparison of methods to discriminate the fluid content of unconsolidated sandstone reservoirs: Geophysics.